



Optics Letters

Accurate optically pumped magnetometer based on Ramsey-style interrogation

DOMINIC HUNTER,*  TERRY E. DYER, AND ERLING RIIS

Department of Physics, SUPA, University of Strathclyde, Glasgow G4 0NG, UK

*Corresponding author: d.hunter@strath.ac.uk

Received 23 November 2021; revised 22 December 2021; accepted 24 January 2022; posted 24 January 2022; published 26 February 2022

Light–atom interactions during spin preparation and readout in optically pumped magnetometers can lead to inaccuracies. We demonstrate a novel, to the best of our knowledge, detection strategy that exploits an interrogation sequence in the pulsed free-induction-decay modality to suppress these systematic errors. The technique is predicated on monitoring the dynamics of preoriented atomic spins as they evolve unperturbed during a dark interval, by subsequently applying a time-delayed optical pulse to infer the spin state’s phase. This detection mode reduced light shift inaccuracies to within 0.6 nT, and could be employed in a wide variety of high-precision atomic magnetometry experiments.

Published by Optica Publishing Group under the terms of the [Creative Commons Attribution 4.0 License](#). Further distribution of this work must maintain attribution to the author(s) and the published article’s title, journal citation, and DOI.

<https://doi.org/10.1364/OL.449180>

Atomic magnetometers demonstrate improved metrological standards compared to many existing technologies and are widely adopted in both fundamental physics experiments and research areas such as space science, geophysics, and medicine [1]. Significant progress has been made since their inception, approaching the fundamental quantum limits in some cases with sub- μT sensitivities [2,3]. This is accredited to recent advancements in optical pumping techniques that enable longer spin coherence lifetimes and improved signal-to-noise ratios (SNRs), e.g., by operating in the spin-exchange relaxation-free (SERF) [4] or light-narrowed [5] regimes. Moreover, developments in microfabricated vapor cell manufacturing processes and the introduction of robust, scalable, inexpensive, tunable diode lasers have established a framework for precision metrology in compact sensor modules [6]. Achieving μT -level precisions with these devices often detrimentally impacts critical performance metrics such as bandwidth, dynamic range, and accuracy. This is particularly evident in SERF vapors which rely on near-zero-field operation and produce narrow resonance linewidths, necessitating both active and passive field compensation [7]. Also, the accuracy of SERF-based sensors is contingent on the magnetic field calibration of the excitation coils which provides an indirect and often inaccurate measurement.

There are many sources of systematic error afflicting optically pumped magnetometers (OPMs), which can be categorized into

two types. The first applies to inaccuracies in extracting the Larmor frequency ω_L during signal analysis. A classic example is commonly observed in closed-loop systems that incur frequency shifts due to phase errors in the feedback signal. Sensors based on the free-induction-decay (FID) mechanism, also known as free spin precession (FSP), are immune to this issue as the precession frequency is monitored directly in the temporal domain. Thus, these sensors are commonly incorporated in experiments searching for the neutron electric dipole moment (nEDM) as the magnetic field can be tracked both precisely and accurately [8,9]. The second type concerns any modifications to the relationship between ω_L and the magnetic field $|\vec{B}|$; this relates to effects that alter the energy separation between Zeeman sublevels, or the distribution of atomic population within the ground-state manifold. For example, there is an accuracy limitation set by quadratic Zeeman splitting which, for Cs, is of the order of 1 nT at Earth’s field [10]. Furthermore, heading errors cause shifts in ω_L attributed to magnetic sublevel populations being redistributed when the sensor orientation is altered [11]. Possibly the most notable contributor to inaccuracies in OPMs is the AC Stark effect (i.e., light shift), which increases with the optical field intensity present during detection. Stark shifts are composed of both vector and tensor components that are often associated with circularly and linearly polarized light, respectively [12]. These shifts are particularly prevalent in cw pump–probe schemes where the alkali vapor is interrogated at high laser intensities [13]. Suppressing light shifts, e.g., technique in Ref. [14], has been instrumental in improving the long-term frequency stability of atomic clocks as the effects of temporal variations in laser power and frequency are reduced. Equivalent methods are yet to be employed in atomic magnetometers.

In this Letter, we present an OPM implementing a novel interrogation mode analogous to Ramsey spectroscopy [15]. This enables observation of spin dynamics without introducing perturbations from external electric fields during detection. In the past, spin lifetimes have been measured using similar readout methods [16] derived from Franzen’s technique of “relaxation in the dark” [17]. The basic principle is predicated on optically pumping an atomic sample into a well-defined quantum state that subsequently evolves during a period of darkness. This is followed by a time-delayed optical pulse that determines the spin phase at the instant readout is initiated. It is possible to reconstruct the evolving spin state by superimposing observations at various delay times, manifesting as precession and

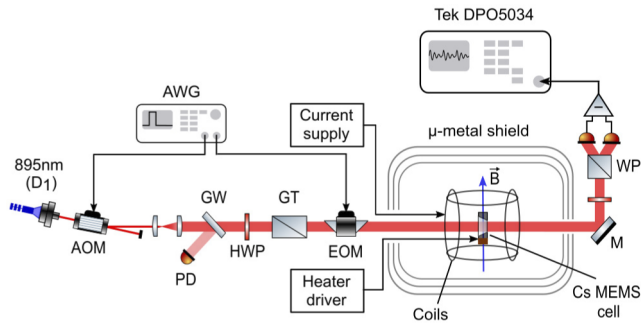


Fig. 1. Simplified experimental setup: AOM, acousto-optic modulator; EOM, electro-optic modulator; GW, glass window; HWP, half-wave plate; GT, Glan–Thompson polarizer; MEMS, micro-electromechanical system; M, mirror; WP, Wollaston prism; PD, photodiode; AWG, arbitrary waveform generator.

partial relaxation of the alkali spins during the dark interval. This phase-sensitive detection strategy offers accurate magnetic field tracking as the AC Stark effect is largely suppressed. Furthermore, residual optical pumping effects that broaden the magnetic linewidth are significantly reduced. This provides a platform for assessing the intrinsic relaxation properties of vapor cells. Compared to previous relaxation studies that extrapolate to zero-light power [18], this method can significantly improve SNR by using elevated laser intensities during readout.

The experimental arrangement is depicted in Fig. 1, comprising an OPM operated in a pulsed FID scheme using a single-beam geometry [19,20]. An extended cavity diode laser (Toptica DL 100) is manually tuned to the Cs D_1 line using an auxiliary reference cell, close to the unresolved $F = 3 \rightarrow F'$ hyperfine transition of the collisionally broadened buffer gas cell. The fiber-coupled output passes through an acousto-optic modulator (AOM) that amplitude-modulates the light beam, with a maximum power of 6 mW. Light shifts are minimal during the dark interval as the remaining optical power is only a few microwatts, limited by the AOM's extinction ratio. The AOM rise time is considerably faster than the atomic absorption rate, which was determined experimentally to reside in the kilohertz range [19]. The width ($1/e^2$ diameter) of the beam's spatial intensity profile was measured to be 1.8 mm. The beam passes through a half-wave plate and Glan–Thompson polarizer to purify the light polarization before traversing an electro-optic modulator (EOM) that switches between circular and linear polarizations for optical pumping and readout, respectively. Laser power is monitored with a calibrated photodiode that assists in edge detection during signal analysis. The sensing element consists of a MEMS Cs vapor cell containing N_2 buffer gas at 165 Torr [19]. The cell temperature was raised to 85°C by passing a gated current through a resistive heating element, with no current applied during detection to improve measurement accuracy by avoiding stray fields. The sensor head was enclosed in a three-layer μ -metal shield nulling ambient fields to nT levels and suppressing magnetic technical noise. A constant current was applied to a set of Helmholtz coils inside the innermost shield, generating a 5 μ T bias field transverse to the light propagation axis. Control voltages to the AOM and EOM were both provided by the same Keysight 33500B series arbitrary waveform generator (AWG). Evolving spin dynamics in the Zeeman manifolds alter the vapor's birefringent properties [19]. This is imprinted in the probe light's polarization which

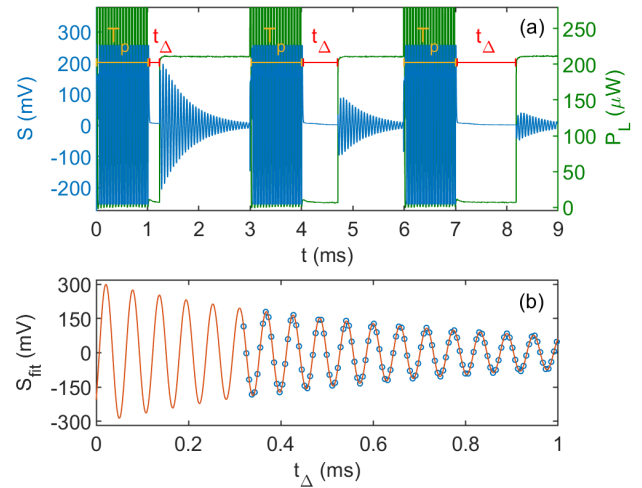


Fig. 2. (a) Subsection of FID signal train (lower curve) and corresponding laser power (upper curve) prior to illuminating the vapor cell. Light intensity is set close to zero for a time t_Δ after optical pumping for $T_p = 1$ ms, followed by a readout stage to infer the spin state. (b) Precession signal (circles) reconstructed “in the dark” using a readout power of 210 μ W over a series of delay intervals. Each point represents the fitted signal amplitude at the point the light was switched on. The associated DS fit (curve) is used to model the spin dynamics unperturbed by optical fields.

is detected by the polarimeter and captured using a Tektronix DPO5034 oscilloscope for post-processing.

Figure 2 demonstrates the principles of the modality discussed in this Letter. The spins are resonantly driven at ω_L by synchronously modulating the laser intensity for a duration T_p [8], extending to at least one relaxation period such that the Cs spins occupy a highly polarized state. After optical pumping, the light–atom interaction is switched off during an interval of darkness t_Δ , permitting the spin coherence to relax and precess freely in the controlled static magnetic field. An optical pulse at a light power of $\approx 210 \mu$ W is applied for readout, subjecting the atoms to various systematics in the process. Interval t_Δ was measured by detecting edges in the monitor photodiode signal, with timing errors limited by clock jitter (<40 ps) in the AWG to which the oscilloscope was synchronized. The resulting phase fluctuations ($<5 \mu$ rad) yield negligible contribution to the sensor's noise floor and accuracy. Figure 2(a) displays the raw oscilloscope data; the upper curve corresponds to the optical power measured before striking the vapor cell, and the lower curve shows FID traces for a preselected subset of delay times. It should be noted that light shifts are still prominent in each FID signal; however, the initial phase of the spin state during readout represents evolution when the light–atom interaction is minimized. By employing an appropriate theoretical model to the precession signal, e.g., damped sinusoid (DS) [19], one can deduct the exact quantum state of the atomic ensemble when the dark period ended.

A low bias field was applied to enable a significant segment of the precession signal to be reconstructed with sufficient time resolution, limited by the sensor's repetition rate and the oscilloscope's buffer size. The FID signal envelopes seen in Fig. 2(a) deviate slightly from the expected exponential behavior. This is caused by the probe light coupling to both hyperfine ground states which have slightly different gyromagnetic ratios

with opposite sign. Optical spectroscopy with the Cs MEMS cell verified that the collisionally broadened optical resonances were resolvable but slightly overlapping [19]. The first $50 \mu\text{s}$ of each FID trace was removed in order to improve the fitting quality. Signal truncation was kept consistent for all data analyses including both the DS fit and the Hilbert transform. FID data deviating from the anticipated DS model present a small source of systematic error influenced by signal characteristics such as SNR, decoherence rate, and truncation. Despite these sources of error, the measurement accuracy still reflects a vast improvement in comparison to the 8 nT fictitious field measured at $210 \mu\text{W}$ in this case. Extrapolating with a DS fit to when readout is initiated allows one to delineate the spin evolution independent of light intensity, by incrementally varying the delay time over subsequent FID cycles. Figure 2(b) shows the first point in the DS fit applied to each FID signal, thus temporally mapping the spin dynamics. The resulting signal is fitted to determine the precession and decoherence rates unaffected by optical fields. It is not necessary to map out the spin evolution in its entirety. The light-shifted FID signals can be used to obtain a close estimate of ω_L , so measuring the spin phase at two different delay times would provide enough information to accurately determine $|\vec{B}|$. Analogous methods using an auto-balanced Ramsey interrogation protocol are employed in atomic clocks [14]. It is anticipated that the frequency response of this sensor would closely align with the behavior presented in Ref. [20], although with an additional scaling to the number of FID cycles used to record $|\vec{B}|$. A single cycle could be used but would be subject to consistency in the spin state generated after optical pumping.

Thus far, data analysis has been limited to fitting the FID signals to a DS model using the Levenberg–Marquardt algorithm as performed in previous instances [19,20]. The validity of this approach was verified with a Hilbert transformation, as both techniques were applied to the FID trace shown in Fig. 3(a). The Hilbert transform $\mathcal{H}\{S(t)\}$ linearizes the signal through retrieval of the instantaneous phase [21]. The signal's analytic representation can be expressed as

$$S_a(t) = S(t) + i\mathcal{H}\{S(t)\}, \quad (1)$$

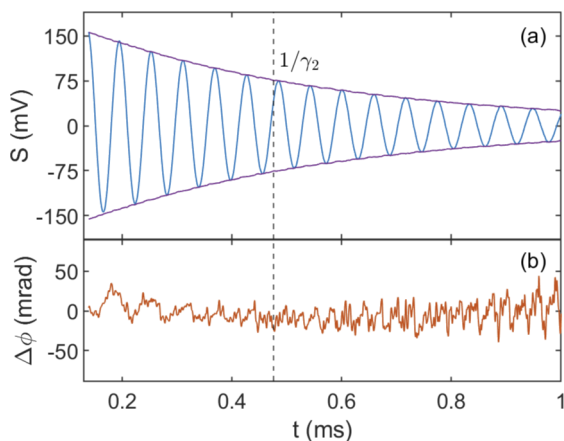


Fig. 3. (a) Raw FID trace (fluctuating curve) and exponential envelope derived by calculating the radius of the phasor $S_a(t)$ in Eq. (1). The dashed line is positioned at one relaxation period $1/\gamma_2$. (b) Signal phase computed with the Hilbert transform subtracted from the accumulated phase ascertained with the DS fit.

where $S(t)$ is the raw trace and $\mathcal{H}\{S(t)\}$ is the $\pi/2$ phase-shifted signal given by

$$\mathcal{H}\{S(t)\} = \frac{1}{\pi} \text{p. v.} \int_{-\infty}^{\infty} \frac{S(\tau)}{t - \tau} d\tau. \quad (2)$$

The instantaneous amplitude and phase can be determined by calculating the radius and angle of $S_a(t)$ in the complex plane. Here ω_L and the starting phase are calculated from the slope and intercept of the linear phase dependence. Figure 3(b) compares the Hilbert transform and DS fit methods by subtracting the instantaneous phases computed with each. The model does not account for higher-order harmonics of ω_L or asymmetries in the signal envelope, hence the oscillatory behavior and a slight second-order dependence. Aside from these small deviations, there is no significant slope in $\Delta\phi(t)$ which is a clear indication that both techniques are closely matched. The FID trace in Fig. 3(a) was truncated after 1 ms as the SNR reduces due to spin decoherence. The signal $\mathcal{H}\{S(t)\}$ does not preserve any DC offsets; a first-order digital high-pass Butterworth filter with a cutoff frequency of 1 kHz removed offsets from the raw data before transformation. The relaxation rate can also be calculated by fitting to the exponential envelope in Fig. 3(a).

Figures 4(a) and 4(b) illustrate the light-shifted fictitious field B_{LS} and power broadening contribution to the relaxation rate γ_{pb} as the readout power is varied. No data were collected below $100 \mu\text{W}$ to maintain an acceptable SNR. It can be seen that B_{LS} and γ_{pb} were computed using both the DS fit and Hilbert transform which, as expected, provide almost identical trends. The observed light shift has a negative slope as the laser frequency was blue-detuned with respect to the $F = 4 \rightarrow F' = 3$ transition. Readout was performed using linearly polarized light

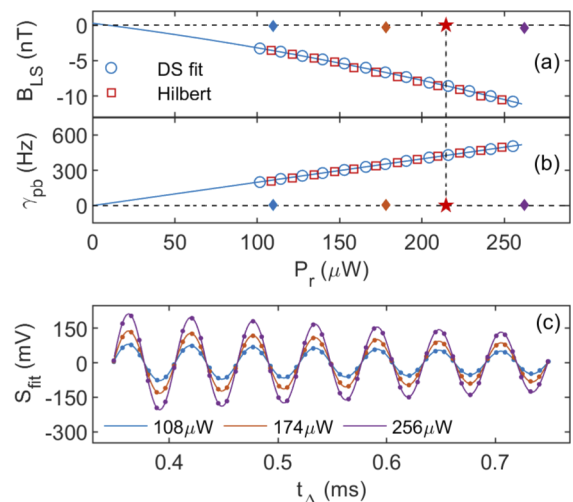


Fig. 4. (a) Fictitious field B_{LS} and (b) deviation from the vapor cell's intrinsic relaxation rate due to power broadening γ_{pb} as a function of readout power. The beam diameter was 1.8 mm . Empirical polynomial models (curves) were applied to the DS fit parameters (circles). Results processed with the Hilbert transform method (squares) are shown for comparison. The precession frequency and decay rate extracted from Fig. 2(b), represented by stars, are consistent with that expected at zero-light power. (c) Reconstructed precession signal (dots) and corresponding fits (solid curves) using readout powers noted in the legend. Variations in B_{LS} and γ_{pb} for the signals in (c) are represented as diamonds close to zero in (a) and (b). All markers are larger than the associated error bars.

which suggests that the fictitious field is generated by the tensor contribution to the light shift [22]. The nonlinear fictitious field dependence with light intensity seen in Fig. 4(a) is likely a result of back-action during readout. The curve in Fig. 4(a) has been extrapolated to zero-light power using an empirical second-order polynomial applied to the DS fit parameters. The star represents the light shift measured from the reconstructed precession signal in Fig. 2(b), and demonstrates good agreement with the empirical model at zero-light power. Figure 4(b) exhibits extensive power broadening contingent on the light-atom interaction strength during readout. Here γ_{pb} was estimated using a DS fit, shown as circles, and also by fitting the exponential envelope obtained through the Hilbert transform, represented by the squares; γ_{pb} displays a clear linear dependence with readout power, and the extrapolated zero-light power value shows excellent agreement with the reconstructed signal in Fig. 2(b). The zero points denoted by the dashed lines in Figs. 4(a) and 4(b) are defined by the offsets in the empirical polynomial fits to ω_L and γ_2 . This verifies the technique's ability to suppress light-induced systematics, which is confirmed further by considering the Larmor frequencies of the reconstructed precession signals in Fig. 4(c). Variations in B_{LS} and γ_{pb} measured from these data sets are denoted by diamonds in Figs. 4(a) and 4(b), respectively. A linear fit was applied to the measured precession frequencies as a function of readout power. The slope was measured to be $(-1.56 \pm 3.06) \text{ pT}/\mu\text{W}$, and the magnetic field (intercept) error was 0.59 nT, defining the accuracy limit imposed by this interrogation strategy. Preliminary experiments indicate comparable sensitivity to the conventional FID scheme. An extensive characterization is subject to further investigation.

In conclusion, a novel detection mode was presented that enables significant suppression of operational systematics imposed by interactions with optical fields. A temporally separated interrogation sequence that involves optical pumping, free precession in the dark, and optical readout is implemented. Insensitivity to light shifts was demonstrated in two ways: the first example shows that ω_L and γ_2 deduced from the precession signal mapped out, "in the dark," were in excellent agreement with the observations made when extrapolating to zero-light power; second, three precession signals were reconstructed at different readout powers, and no perceivable trend in ω_L and γ_2 was evident. Systematics relating to inaccuracies in signal analysis exist as the DS fit model contains only a single frequency component. This is a simplification as we are interacting with both collisionally broadened hyperfine ground states simultaneously, which oscillate at slightly different frequencies with opposite phase. The fitting quality can be improved by: adapting the model to take into account both frequency components, tuning the laser wavelength such that we are mostly interacting with a single ground-state transition, or emptying atomic population from the $F = 3$ ground state with a second repump beam and probing the $F = 4 \rightarrow F'$ transition. The latter two options are preferable as they reduce the signal complexity that, in turn, simplifies parameter extraction. It is not unreasonable to assume that these improvements could lead to accuracies that closely match the instrument's own precision. Such unprecedented accuracy and low drift operation would be ideal for long-term magnetic field monitoring, e.g., in geophysical surveys, nEDM searches, or GPS-denied navigation. Moreover, the absence of power broadening is ideal for measuring relaxation properties intrinsic

to the vapor cell with high fidelity. This would be extremely useful for cell characterization before deployment in compact sensor modules, and could even be implemented at a wafer level.

Funding. Engineering and Physical Sciences Research Council (EP/T001046/1).

Acknowledgments. The authors would like to thank Dr. Stuart J. Ingleby and Dr. Paul F. Griffin for many valuable discussions.

Disclosures. The authors declare no conflicts of interest.

Data availability. Data underlying the results presented in this paper are available in Ref. [23].

REFERENCES

- D. Budker and D. F. J. Kimball, *Optical magnetometry* (Cambridge University Press, 2013).
- W. E. Bell and A. L. Bloom, *Phys. Rev. Lett.* **6**, 280 (1961).
- H. Dang, A. C. Maloof, and M. V. Romalis, *Appl. Phys. Lett.* **97**, 151110 (2010).
- J. Allred, R. Lyman, T. Kornack, and M. V. Romalis, *Phys. Rev. Lett.* **89**, 130801 (2002).
- S. Appelt, A. B.-A. Baranga, A. Young, and W. Happer, *Phys. Rev. A* **59**, 2078 (1999).
- S. Knappe, P. Schwindt, V. Gerginov, V. Shah, L. Liew, J. Moreland, H. Robinson, L. Hollberg, and J. Kitching, *J. Opt. A: Pure Appl. Opt.* **8**, S318 (2006).
- S. J. Mellor, T. M. Tierney, G. C. O'Neill, N. Alexander, R. A. Seymour, N. Holmes, J. D. López, R. M. Hill, E. Boto, M. Rea, G. Roberts, J. Leggett, R. Bowtell, M. J. Brookes, E. A. Maguire, M. C. Walker, and G. R. Barnes, *bioRxiv* (2021).
- Z. D. Grujić, P. A. Koss, G. Bison, and A. Weis, *Eur. Phys. J. D* **69**, 135 (2015).
- S. Afach, G. Ban, and G. Bison, *et al.*, *Opt. Express* **23**, 22108 (2015).
- S. Seltzer, P. Meares, and M. Romalis, *Phys. Rev. A* **75**, 051407 (2007).
- G. Bao, A. Wickenbrock, S. Rochester, W. Zhang, and D. Budker, *Phys. Rev. Lett.* **120**, 033202 (2018).
- B. Mathur, H. Tang, and W. Happer, *Phys. Rev.* **171**, 11 (1968).
- V. Schultze, B. Schillig, R. IJsselsteijn, T. Scholtes, S. Woetzel, and R. Stolz, *Sensors* **17**, 561 (2017).
- M. Shuker, J. Pollock, R. Boudot, V. Yudin, A. Taichenachev, J. Kitching, and E. A. Donley, *Phys. Rev. Lett.* **122**, 113601 (2019).
- N. F. Ramsey, *Phys. Rev.* **78**, 695 (1950).
- M. Shuker, O. Firstenberg, Y. Sagi, A. Ben-Kish, N. Davidson, and A. Ron, *Phys. Rev. A* **78**, 063818 (2008).
- W. Franzen, *Phys. Rev.* **115**, 850 (1959).
- T. Scholtes, S. Woetzel, R. IJsselsteijn, V. Schultze, and H.-G. Meyer, *Appl. Phys. B* **117**, 211 (2014).
- D. Hunter, S. Piccolomo, J. Pritchard, N. Brockie, T. Dyer, and E. Riis, *Phys. Rev. Appl.* **10**, 014002 (2018).
- D. Hunter, R. Jiménez-Martínez, J. Herbsommer, S. Ramaswamy, W. Li, and E. Riis, *Opt. Express* **26**, 30523 (2018).
- N. Wilson, C. Perrella, R. Anderson, A. Luiten, and P. Light, *Phys. Rev. Res.* **2**, 013213 (2020).
- Y. Jia, Z. Liu, M. Ding, Z. Chai, X. Liang, and W. Wu, *Appl. Phys. Lett.* **116**, 142405 (2020).
- D. Hunter, Terry E. Dyer, and E. Riis, "Data for: An accurate optically pumped magnetometer based on Ramsey-style interrogation," University of Strathclyde, (2021) <https://doi.org/10.15129/a79c7e5f-0a41-4f6a-a9f2-393409a71488>.